Hybrid Wireless Positioning

Marco Vihelmo Velapatino Gamarra
ma7271ve-s@student.lu.se

Phalguni Nagendra
ph0061na-s@student.lu.se

Department of Electrical and Information Technology

Lund University

Supervisor: Fredrik Tufvesson (EIT)

Company supervisor: Peter Karlsson (u-blox, Malmö)

Examiner: Maria Kihl (EIT)

October 2022

Printed in Sweden
Tryckeriet i E-huset, Lund

Abstract

Numerous location-based services (LBS) have evolved because of the fast development of mobile Internet for use in commerce, entertainment, security, and other areas. All of these need a precise real-time location-based service with smooth indoor-outdoor transition in highly populated areas. A truly omnipresent location system for both indoor and outdoor settings is still not accessible, despite the global navigation satellite system (GNSS) technology enabling excellent outdoor location services. To find a solution for the indoor-outdoor transition accuracy, we suggest a solution of hybrid positioning system (HPS) that combines the position data of Bluetooth Low Energy (BLE) Beacon and the GNSS technology. This work investigates a BLE-GNSS Hybrid positioning scheme based on AOA (Angle of Arrival) obtained by BLE and GNSS position estimate. The fusion algorithms tested here are the Weighted-Least square (WLS) method and the Kalman filter (KF) method. At the end of the investigation, we draw a comparison between these two fusion algorithms, and the results in the indoor-outdoor environment show that the proposed solution based on WLS improves the accuracy by up to 22% while the one based on KF enhances the accuracy by up to 38% compared to BLE performance, in the same environment the performance is improved compared with GNSS, HPS based on Kalman filter improves the accuracy up to 62% and HPS based in WLS improves the accuracy up to 31%.

Keywords: Global Navigation Satellite System (GNSS), Bluetooth Low Energy (BLE), Hybrid Positioning System (HPS), Fusion Algorithms.

Popular Science Summary

Currently, there is a great interest in location-based applications. These applications are used in industry, academia, and society. Not only has the demand for location systems grown, but these services also need to be very accurate in their estimates and be able to function well in different scenarios. These scenarios can be outdoor, indoor, or a combination of them. Most current location technologies have optimal performance in a specific scenario, such as GPS, which is typically a very reliable and accurate radio navigation system in outdoor scenarios, however, the use of GPS in indoor scenarios is affected by the loss of visibility of the devices with the satellites and the loss of signal due to obstacles such as walls or floor levels. On the other hand, there are solutions for indoor locations which include technologies such as Bluetooth, Wi-Fi, and RFID among others. These technologies can be found in almost all current mobile devices. Among these technologies, Bluetooth stands out due to its low energy consumption and the feature Direction Finding that is included in Bluetooth 5.1. This feature allows the equipment to determine the direction of a signal through different methods such as Angle of Arrival (AoA). The use of this characteristic allows the development of accurate indoor location applications based on Bluetooth.

Although the different technologies mentioned above have good performance in specific environments, the use of position-based applications is not restricted to a single scenario, so it is necessary to have a system that can give an accurate location regardless of where the user is. A hybrid Positioning System (HPS) is presented as an alternative to cover this need. HPSs make use of two or more technologies to obtain a more accurate position estimate. In this work, the possibility of using GPS and Bluetooth direction finding based on AoA as components of a HPS is studied, for which different methods are investigated and tested to combine the position estimates given by the components of the HPS and thus, obtain a better estimate of the final position in indoor-outdoor scenarios.

Acknowledgement

First and foremost, we would like to express our gratitude to u-blox for their cooperation in producing this master's thesis. We have greatly valued the chance to learn more about your work and participate in the technology solutions you develop.

We especially like to thank Peter Karlsson our supervisor at u-blox for all the time and assistance you have provided us with over the entire thesis duration. I appreciate your explanations, fresh suggestions, and ongoing assistance.

We would like to express our gratitude to our supervisor Fredrik Tufvesson and our examiner Maria Kihl at Lund University for their direction and help during our project.

Also, we would like to thank everyone in u-blox positioning team Farshid Rezaei, Stelios Papaharalabos, Mohammad Abu Nasa, and Yannick Stebler for their continued assistance. Your help has really been appreciated!

Table of Content

List of Abbreviations

FP	fingerprint
RSS	Received Signal Strength
RSSI	Received Signal Strength Indicator
GPS	Global Positioning System
HLS	Hybrid Location System
PDS	Pedestrian Dead Reckoning
AoA	Angle of Arrival
UWB	Ultra Wide Band
UE	User Equipment
HPS	Hybrid Positioning System
AP	Anchor Points
ISM	Industrial, Science and Medical
SIG	Special Interest Group
FHSS	Frequency Hopping Spread Spectrum
BR/EDR	Basic Rate/Enhanced Data Rate
GFSK	Gaussian Frequency Shifting
GLONASS	Globalnaya Navigazionnaya Sputnikovaya Sistema
PNT	Position, Navigation and Time
PCB	Printed Circuit Board
SV	Satellite Vehicle
DOP	Dilution of Precision
HDOP	Horizontal Dilution of Precision
VDOP	Vertical Dilution of Precision
PDOP	Positional Dilution of Precision
GDOP	Geometrical Dilution of Precision
RTK	Real-Time Kinematics
PPP	Precision Point Positioning
SPP	Single Point Positioning
LOS	Line of Sight
ECEF	Earth Centered Earth Fixed
ENU	East-North-Up
UERE	User Equivalent Range Error
LS	Least Square
WLS	Weighted Least Square
KLF	Kalman Filter

IQ	Inphase and Quadrature
MUSIC	MUltiple SIgnal Classification
PDDA	Push Different Data Algorithm
GT	Ground Truth
PVT	Position Velocity Time
PR	Pseudo Range
CDF	Cumulative Distributive Frequency

Chapter 1

Introduction

Currently there is a great demand for the use of location applications, both from end users and from the industry, mainly in the automotive industry. This demand is growing and due to the use, that is given to them, it is necessary to have applications that work with the best possible accuracy. The applications make use of different technologies to obtain position estimates such as Wi-Fi, GNSS, BLE, etc. These positioning technologies have acceptable performance under specific conditions. So, their use is restricted to certain environments (indoor, outdoor, etc.). However, the places where these applications are used are usually not always restricted to a single environment, the use can occur in a combination of these (urban, suburban environments, etc.) for which location technologies are needed to have the best performance in every environment. Hybrid Positioning systems (HPS) combine the use of two or more technologies to improve location accuracy. Due to these characteristics, HPS are presented as a suitable system to be used in applications that are used in different environments.

In recent years, several works related to hybrid location systems for indoor-outdoor environments have been carried out, mainly due to the need to improve location accuracy. In [1], a hybrid location system is proposed that merges the multilateration (MLT) and fingerprinting (FP) methods based on Bluetooth Low Energy (BLE) Beacons; the results show an improvement in the accuracy of the position obtained by the hybrid system compared to individual methods, tests were however performed only in indoor environments. In the same way, works have been done where different technologies are merged in indoor-outdoor environments. In [2], Wi-Fi fingerprinting was used as part of the hybrid system, however the use of Wi-Fi fingerpainting based on received signal indicator (RSSI) requires a site survey to identify the access points and their positions, which leads to a great effort and expense of resources. In [3] a hybrid system based on GPS and Wi-Fi is proposed that obtains access points more efficiently compared to [2] by means of pedestrian dead reckoning (PDR). In most of the works done before where BLE is part of Hybrid solution the position is estimated by applying RSS received [4]. In this work the position estimation of the BLE device will be estimated by using the angle of arrival of the signal (AoA) this is a new feature included in Bluetooth Low Energy (BLE). In [5], UWB and GPS technology are used as part of a hybrid location system. The system proposed was tested using simulated data. In the mentioned works, it is verified that the use of Hybrid systems for location improves the

precision, however, few works have been implemented where BLE and GNSS technology are merged in indoor-outdoor environments, even though the use of BLE for location can exceed Wi-Fi as shown in [6] and that both BLE and GNSS are ubiquitous in indoor and outdoor environments respectively.

1.1. Background

The Global Navigation Satellite System (GNSS) refers to a constellation of satellites that provide signals through space which transmit positioning and timing data to GNSS receivers. These received data are then used to determine the location [7]. GNSS is used to estimate the position of wireless devices (UE's), but by fact we know that the hindrance can be observed due to a lot of factors like buildings, low visibility, or indoor-outdoor facilities etc. Since the global navigation satellite system (GNSS) is not available indoors, research has been focused on alternative wireless technologies, one of which is the Bluetooth Low Energy (BLE). To improve the accuracy, we are adopting a hybrid wireless positioning approach, for which Bluetooth Low Energy is used. BLE is a form of wireless communication designed especially for short-range communication. BLE is very similar to Wi-Fi in the sense that it allows devices to communicate with each other. However, BLE is meant for situations where battery life is preferred over high data transfer speeds. Here the results are mainly obtained focusing on the Angle of Arrival (AoA), and the BLE with GNSS reading integration has shown some of the positive and promising results for the hybrid solution [9].

1.2. Purpose

The main aim of this project is to investigate methods to improve location accuracy in indoor-outdoor environments (overlapped area) using a hybrid location system. Since the location accuracy in this transition environment decreases when using separate location technologies such as GNSS or Bluetooth. To improve the position accuracy in indoor-outdoor environments a fusion method will be used to merge BLE and GNSS position data estimates.

To achieve this aim, we will test two fusion methods: Weighted Least Square, and Kalman Filters. In these tests, position estimates will be used which will be obtained using BLE and GNSS technologies. These technologies are widely used in indoor and outdoor location respectively.

This work intends to answer the following questions:

- How do WLS and KF fusion methods work?

- Which fusion method is more accurate?
- Are WLS and KF fusion methods able to improve the position accuracy compared with BLE and GNSS technologies alone?

1.3. Methodology

To investigate the hybrid location system, GNSS and BLE technologies will be studied first, in addition to sensor fusion methods. In this way, we will be able to identify the most appropriate parameters of each technology so that they can be used in the studied fusion algorithms. The fusion algorithms will be implemented based on MATLAB code. These implementations will be tested with two sets of data. The first fusion test is performed with real BLE and GNSS simulated data. To obtain simulated GNSS data, the company U-Blox's Navlab simulator is used, and in the case of BLE, the data will be obtained from several field tests in indoor-outdoor environments. In the second test, real positioning measurements are made in a suburban environment using the XPLR-IOT-1 device from the company U-Blox which can obtain its position using BLE and GNSS independently; the data obtained in the field tests are merged using fusion methods. Finally, a comparison of the performance between the fusion method and the BLE and GNSS technologies is made.

1.4. Report structure

The thesis report is divided into five chapters:

Chapter 2 delivers the theoretical background of various fields that are required for the development of this thesis. Here, we start with describing BLE, how it evolved, its applications, and how indoor position reading is obtained using BLE which eventually talks about the tags and the AP (anchor points) used to collect the position estimate data. Later, it covers a detailed explanation of the Global Navigation Satellite System (GNSS). Three different types of fusion algorithms are described. The last section describes the Angle of Arrival (AoA).

Chapter 3 presents the measurement setup in the field tests. It explains Bluetooth data acquisition, GNSS data acquisition, measurement setup and hybrid Fusion algorithms. The three different scenarios i.e., Indoor, Outdoor, and Indoor-Outdoor are discussed. And fusion methods are investigated.

Chapter 4 provides results that were acquired to answer the questions, as well as the various factors that influenced the outcome. The chapter investigates fusion algorithms for all three scenarios.

Chapter 5 presents the analysis of the result obtained in the field test.

Chapter 6 is the conclusion, describing which technology gives the better estimate of position and comparison between stand alone technologies and Hybrid technologies. Also, the future research and implementations that are going to happen in the field of hybrid wireless positioning, where different technologies and scenarios will be considered.

1.5. Limitations

This work focuses on analyzing the performance of two fusion methods. This analysis is based on the comparison between the error in the position obtained by the studied methods and the BLE and GNSS technologies. The performance of the studied solutions is strongly affected by measurement uncertainties, which in turn depend on the equipment used and the environmental factors under the tests were performed. The results presented in this work were obtained under specific conditions described in the following chapters and they cannot be generalized. The solutions based on the methods under study might be viewed as proof of concept on which future research can be developed.

Chapter 2

Theoretical Background

2.1. Bluetooth Low Energy

An ultra-compact Bluetooth beacon is a Bluetooth Low Energy-based wireless gadget. Similar to a lighthouse, it continuously transmits a signal that other devices can detect. But instead of producing visible light, it sends out a radio signal that consists of a mix of letters and numbers that are broadcast at brief, regular intervals. A Bluetooth-equipped device such as a smartphone, gateway, or access point may "see" a beacon once it comes within range. Figure 1 shows the basic operation of the BLE Beacon [10]. The Bluetooth Basic Rate/Enhanced Data Rate (BR/EDR) operates in the Industrial, Scientific, and Medical (ISM) radio band whose frequencies range from 2.4 GHz to 2.48 GHz and makes use of 79 channels within this band. It also uses Frequency-hopping Spread Spectrum (FHSS) to jump between channels. Bluetooth Special Interest Group (SIG) manages this technology and oversees its development, licensing, and trademarking [11]. Bluetooth Low Energy (BLE) is a new version of this technology that has improvements in energy consumption and location applications. BLE uses 40 channels in the unlicensed frequency band ISM as well as GFSK as a modulation technique, but its most outstanding feature is BLE direction finding, which with the help of an array of antennas can calculate the direction of a received signal. Table.2.1. shows the differences between Bluetooth Classic and Bluetooth low Energy.

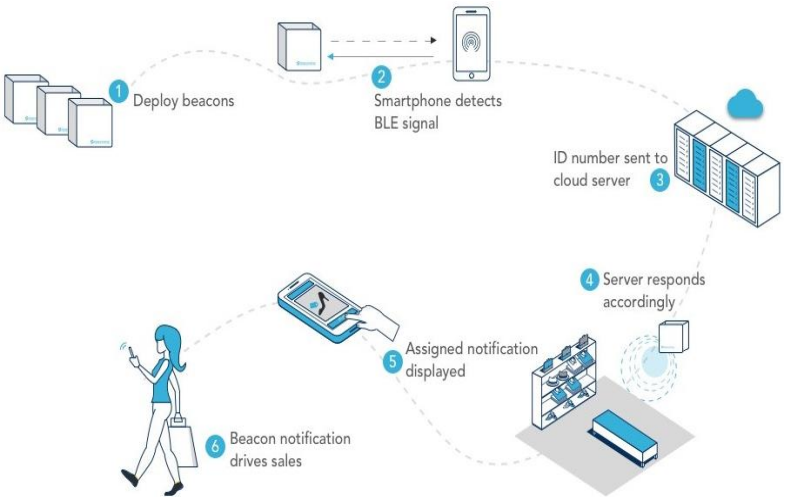

Figure 2.1: Basic working of BLE beacon **[11]**

	Bluetooth Low Energy (LE)	Bluetooth Classic
Frequency Band	2.4GHz ISM Band (2.402 – 2.480 GHz Utilized)	2.4GHz ISM Band (2.402 – 2.480 GHz Utilized)
Channels	40 channels with 2 MHz spacing (3 advertising channels/37 data channels)	79 channels with 1 MHz spacing
Channel Usage	Frequency-Hopping Spread Spectrum (FHSS)	Frequency-Hopping Spread Spectrum (FHSS)
Modulation	GFSK	GFSK, π/4 DQPSK, 8DPSK
Data Rate	LE 2M PHY: 2 Mb/s LE 1M PHY: 1 Mb/s LE Coded PHY (S=2): 500 Kb/s LE Coded PHY (S=8): 125 Kb/s	EDR PHY (8DPSK): 3 Mb/s EDR PHY (π/4 DQPSK): 2 Mb/s BR PHY (GFSK): 1 Mb/s
Tx Power	≤ 100 mW (+20 dBm)	≤ 100 mW (+20 dBm)
Rx Sensitivity	LE 2M PHY: ≤-70 dBm LE 1M PHY: ≤-70 dBm LE Coded PHY (S=2): ≤-75 dBm LE Coded PHY (S=8): ≤-82 dBm	≤-70 dBm
Data Transports	Asynchronous Connection-oriented Isochronous Connection-oriented Asynchronous Connectionless Synchronous Connectionless Isochronous Connectionless	Asynchronous Connection-oriented Synchronous Connection-oriented
Communication Topologies	Point-to-Point (including piconet)	Point-to-Point (including piconet)
	Broadcast	
	Mesh	
Positioning Features	Presence: Advertising Direction: Direction Finding (AoA/AoD) Distance: RSSI, HADM (Coming)	None

Table 2.1: Differences between BLE and Bluetooth Classic **[12]**

2.1.1. Angle of Arrival (AoA)

The Angle of Arrival is based on the notion of determining angular directions (Azimuth and Elevation) from a device (also known as a Locator) placed at a known location. The angle at which the signal meets the receiver is referred to as the angle.

The phase of the receiving radio signals is used to calculate the angle [13]. A network-centric architecture based on an angular estimate is a position calculation based on the Angle of Arrival (AoA). In contrast to lateration, a Bluetooth device can send direction-finding-enabled packets using a single antenna to reveal its location. The radio signal is subsequently received by the Locator, which is a multi-antenna device. Two angles computed from a Locator are required for a two-dimensional identification of a point. The position of at least two Locators is triangulated for three-dimensional identification [13].

2.2. Global Navigation Satellite System (GNSS)

The Global Navigation Satellite System (GNSS), which provides precise and dependable localization, is widely used in people's lives. However, using GNSS signals for locating in difficult propagation situations such as urban and interior scenarios, where effects such as blocking and multipath are prevalent, is still a work in progress [14]. The definition of GNSS is the technical interoperability and compatibility of various satellite navigation systems, such as modernized GPS, Galileo, and reconstructed GLONASS, to be used by civilian users without regard to the nationalities of each system in order to improve the safety and convenience of life. The concept of a navigation reference system is critical because all GNSS applications are linked to the coordinate system utilized. The major application of GNSS is to calculate the position in the Global reference system in a simple, fast, and cost-effective manner anywhere on the globe at any time. The Global Navigation Satellite System (GNSS) is made up of three key satellite technologies: GPS, Glonass, and Galileo. Each one is made up of three sections: a space segment, a control segment, and a user segment. In the three satellite technologies that make up the GNSS, these parts are essentially identical [15].

2.2.1. Satellite Positioning

An artificial satellite constellation that can provide geo-specific locations everywhere in the world is known as a satellite navigation system. Small electronic receivers can compute their position with the highest level of accuracy using this approach, including their latitude, longitude, and height above mean sea level. The framework is useful for establishing a position. Additionally, the signals allow the electronic receiver to precisely determine the current local time, enabling time synchronization. These uses are often referred to as positioning, navigation, and timing (PNT). The usefulness of the location information can be improved by these developments, even if satellite navigation systems operate independently of any telephone [16].

2.2.2. Constellation, Visibility and Availability of Satellites

An antenna and often a separate printed circuit board (PCB) receiver are features of every GNSS receiver. Data from the satellites in the numerous constellations is the only thing these systems do. The signals that are being received by the receivers are essentially orbital data about the satellite vehicle (SV) that delivered the signal and its time of transmission. We can calculate the distance if we know how long it took for the transmitted signal from the satellite vehicle (SV) to reach our antenna on the mower and how quickly data is sent across space. We may begin to establish our position if we have many of these ranges from SVs somewhere in the sky (those of us are old enough to recall how happy we were to see five SVs on an early GPS device). When discussing GNSS constellations and establishing location, it's also important to consider the geometry of how these SVs are positioned in relation to one another. The SVs should be evenly spaced out over the sky for good geometry. If all of the SVs "in view" of the mower is to one side, this is considered bad geometry and is referred to as the "dilution of precision" (DOP). We also invest a lot of time in discussing how these systems' accuracy is declining. The changes in our estimation of the "speed" with which the signal went from the SV to our antenna are one of the main factors we consider. These SVs are circling the planet at a height of about 25,000 and 30,000 kilometers. They send signals that pass through a variety of "space" levels. We must comprehend the variations in transmission speed caused by the ionosphere, the troposphere, satellite clock inaccuracies, receiver clock errors, any mistakes within the projected position provided for the SV, etc [17]. Sharing a multi-constellation signal has many advantages. Multi-constellation integrated positioning has the potential to significantly improve positioning accuracy due to the increased number of visible satellites and improved distribution of satellite skies, especially when positioning is performed in areas where GNSS signals are blocked. Yes, improved satellite visibility can also reduce blind areas for GNSS services caused by terrain, buildings, tree shadows, and satellite outages. Moreover, high measurement redundancy can increase the reliability of the position solution. Therefore, many efforts have been made to study the advantages of multi-constellation integration, such as multi-GNSS real-time kinematics (RTK) positioning, precision point positioning (PPP), and Single Point Positioning (SPP). Most research works were based on datasets from dozens or multiple stations covering a limited range of latitude and longitude. For satellite-based positioning techniques, satellite visibility and positional dilution of accuracy (PDOP) can be used as important metrics to evaluate performance [18].

2.2.3. Pseudorange

The pseudorange is a rough estimate of how far a satellite is from a GNSS receiver. The ranges of (at least) four satellites as well as their positions at the time that their positional data were transmitted will be attempted to be measured by a GNSS

receiver. Each position can be determined at any moment using the satellites' orbital data from the almanac in the message.

The time it takes for each signal to arrive at the receiver is multiplied by the speed of light to determine each satellite's pseudorange. However, the term "pseudorange" is employed since there will unavoidably be accuracy flaws in the time measured. In a GNSS receiver, the time of the clock is used to estimate the distances to multiple satellites at once, and all the calculated distances have the same inaccuracy. Pseudoranges are ranges with the same inaccuracy. The temporal inaccuracy can also be calculated by determining a fourth satellite's pseudorange. [19].
The general pseudorange calculation equation is given by,

$$p = \rho + dp + c(dt - dT) + d_{ion} + d_{trop} + \in_{mp} + \in_{p}, \quad (2.1)$$

where: p = pseudorange measurement

ρ = true range

dp = satellite orbital errors

c = speed of light

dt = satellite clock offset from GPS time

dT = receiver clock offset from GPS time

d_{ion} = ionospheric delay

d_{trop} = tropospheric delay

$\in_{mp}$ = multipath

$\in_{p}$ = receiver noise

2.2.4. Shadowing

Even in the age of smartphones and smart devices, positioning accuracy (of about 5 meters) can be annoying and misleading when used for navigation in cities. Due to a lack of direct line-of-sight (LOS) signals from GNSS satellite constellations, GNSS positioning accuracy is subpar. Our cellphones and navigational systems are compelled to employ multipath signals in the absence of direct signals. Although there are several techniques that partially or completely ignore multipath signals or employ corrections, the accuracy is still not on par with LOS signal availability. Even though using GLONASS in addition to GPS greatly increases the availability of LOS signals, signal geometry issues will still be an issue [20].

2.2.5. Co-ordinate system

Earth Centered Earth Fixed (ECEF): The coordinates' origin for the earth is often set to be in the planet's center. The positive Z axis then departs from the north pole. The equatorial plane will be the X-Y plane. Along the prime meridian is the X-Axis (zero point of longitude). The system is then made right-handed by adjusting the Y axis. It is now in the Indian Ocean, according to this. The majority of satellite systems identify an earth position by using these ECEF (Earth Centered, Earth Fixed) coordinates. This is done because it provides accurate data without requiring the selection of a particular ellipsoid. All that is required is the axis' orientation and the earth's center. More details are required in order to convert to angular coordinates. To prevent further inaccuracy, some high-precision applications are still included in ECEF. Both angular and ECEF coordinates for high accuracy geodetic benchmarks are included in the databases [21]. Figure 3. Represents the ECEF coordinate system.

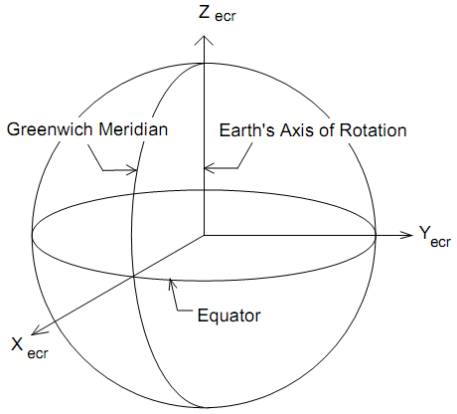

Figure 2.2: ECEF Co-ordinate system **[21]**

East-North-Up co-ordinate system: An east-north-up (ENU) system uses the Cartesian coordinates (xEast, yNorth, zUp) to represent position relative to a local origin. The local origin is described by the geodetic coordinates (lat0, lon0, h0). Note that the origin does not necessarily lie on the surface of the ellipsoid [22].

- The positive *xEast*-axis points east along the parallel of latitude containing *lat0*.
- The positive *yNorth*-axis points north along the meridian of longitude containing *lon0*.
- The positive *zUp*-axis points upward along the ellipsoid normal.

ECEF to ENU transformation:

The relation between the local East, North, Up (ENU) coordinates and the (x, y, z) Earth Centered Earth Fixed (ECEF) coordinates is illustrated in the figure 6. It follows that the ENU coordinates can be transformed to (x, y, z) ECEF by two rotations, where ϕ and λ are, respectively, the latitude and longitude of the ellipsoid: [23]

1.A clockwise rotation over east-axis by an angle $90 - \varphi$ to align the up-axis with the z-axis. That is $R_1[-\left(\frac{\pi}{2}\right) - \varphi)]$.

2.A clockwise rotation over the z-axis by an angle $90 - \lambda$ to align the east-axis with the x-axis. That is $R_3[-\left(\frac{\pi}{2}\right) + \lambda)]$.

That is:

$$\begin{bmatrix} x \\ y \\ z \end{bmatrix} = R_1[-\left(\frac{\pi}{2}\right) - \varphi)]\ R_3[-\left(\frac{\pi}{2}\right) + \lambda)] \begin{bmatrix} E \\ N \\ U \end{bmatrix} \tag{2.2}$$

where, according to the expressions (2)

$$R_1[\theta] = \begin{bmatrix} 1 & 0 & 0 \\ 0 & \cos\theta & \sin\theta \\ 0 & -\sin\theta & \cos\theta \end{bmatrix}; R_2[\theta] = \begin{bmatrix} \cos\theta & 0 & -\sin\theta \\ 0 & 1 & 0 \\ \sin\theta & 0 & \cos\theta \end{bmatrix};$$
$$R_3[\theta] = \begin{bmatrix} \cos\theta & \sin\theta & 0 \\ -\sin\theta & \cos\theta & 0 \\ 0 & 0 & 1 \end{bmatrix} \tag{2.3}$$

This gives,

$$R_3[-\left(\frac{\pi}{2}\right) + \lambda)]R_1[-\left(\frac{\pi}{2}\right) - \varphi)] = \begin{pmatrix} -\sin\lambda & -\cos\lambda\sin\varphi & \cos\lambda\cos\varphi \\ \cos\lambda & -\sin\lambda\sin\varphi & \cos\varphi\sin\lambda \\ 0 & \cos\varphi & \sin\varphi \end{pmatrix}. \tag{2.4}$$

The unit vectors in local East, North and Up directions as expressed in ECEF cartesian coordinates are given by the columns of matrix (2.4). That is:

$$\hat{e} = (-\sin\lambda, \cos\lambda, 0),$$
$$\hat{n} = (-\cos\lambda\sin\varphi, -\sin\lambda\sin\varphi, \cos\varphi),$$
$$\hat{u} = (\cos\lambda\cos\varphi, \cos\varphi\sin\lambda, \sin\varphi). \tag{2.5}$$

Now, Changing this from ECEF to ENU coordinates

Taking into account the properties of the rotation matrices $R_i(\alpha)$, i.e.,

$R_i{}^{-1}(\alpha) = R_i(-\alpha) = R_i{}^{T}(\alpha)$,

$$\begin{bmatrix} E \\ N \\ U \end{bmatrix} = R_1[\left(\frac{\pi}{2}\right) - \varphi)]\ R_3[\left(\frac{\pi}{2}\right) + \lambda)] \begin{bmatrix} x \\ y \\ z \end{bmatrix}, \tag{2.6}$$

Hence the transformation of matrix (2.6) becomes the transpose of matrix (2.4)

$$R_1[\left(\frac{\pi}{2}\right) - \varphi)]R_3[\left(\frac{\pi}{2}\right) + \lambda)] = \begin{pmatrix} -\sin\lambda & \cos\lambda & 0 \\ -\cos\lambda\sin\varphi\cos\lambda & -\sin\lambda\sin\varphi & \cos\varphi \\ \cos\lambda\cos\varphi & \cos\varphi\sin\lambda & \sin\varphi \end{pmatrix}. \tag{2.7}$$

Finally, the ENU coordinates are expressed as,

$$\hat{x} = (-\sin\lambda, -\cos\lambda\sin\varphi, \cos\lambda\cos\varphi),$$
$$\hat{y} = (\cos\lambda, -\sin\lambda\sin\varphi, \cos\varphi\sin\lambda),$$
$$\hat{z} = (0, \cos\varphi, \sin\varphi). \tag{2.8}$$

2.2.6. GNSS Error

The pseudorange between satellites and receivers is the foundation for the Global Navigation Satellite System (GNSS) location. Large position mistakes can emerge from even the tiniest timing problems; for instance, a 10 ns timing error may indicate a 3m pseudorange error.

Ionospheric and Tropospheric Errors: In the ionosphere, Ions with an electrical charge are present. The GNSS signal interacts with these ions as it travels through this layer, slowing it down and causing an error. The troposphere, on the other hand, is the layer that is closest to the surface of the earth. Depending on where on the Earth's surface you are, it is between 8 and 14 kilometers deep. Changes in temperature, density, pressure, or humidity are the causes of tropospheric errors.

Satellite Clock Errors: Even though GNSS satellites are equipped with the most accurate atomic clocks, with nanosecond precision, clock drift can still result in slight mistakes that can influence orientation.

Ephemeris Data Error: These are inaccuracies brought on by the position of the satellite. The mismatch between a GNSS satellite's predicted and actual orbital location is known as an "ephemeris error." Orbital error lowers GNSS accuracy because GNSS receivers utilize the satellite's position in pseudorange computations.

Dilution Of Precision (DOP): The relative locations of the satellites used to derive a position in three-dimensional space may contribute to DOP inaccuracy. It is frequently helpful to apply the notion of Geometrical DOP (GDOP) to have a better understanding. Poor GDOP readings indicate "poor" satellite placement. On the other hand, "well" dispersed satellites yield positive results.

Apart from these errors, there are also errors that can be found in the receiver and also due to multipath. The below figure shows the sources of errors and their range of effect.[24]

Segment Source	Error Source	1σ Error(m)
Space/control	Broadcast clock	1.1
	Broadcast ephemeris	0.8
User	Residual ionospheric delay	0.1
	Residual tropospheric delay	0.2
	Receiver noise and resolution	0.1
	Multipath	0.2
System UERE	Total (RSS)	1.4

Table 2.2: GPS Precise Positioning Service Typical UERE Budget [25].

Segment Source	Error Source	1σ Error(m)
Space/control	Broadcast clock	1.1
	L1 P(Y)-L1 C/A group delay	0.3
	Broadcast ephemeris	0.8
User	Ionospheric delay	7.0*
	Tropospheric delay	0.2
	Receiver noise and resolution	0.1
	Multipath	0.2
System UERE	Total (RSS)	7.1*

Table 2.3: GPS Standard Positioning Service Typical UERE Budget [25].

*Note that residual ionospheric errors tend to be highly correlated among satellites resulting in position errors being far less than predicted using DOP · UERE User equivalent range error [25].

2.2.7. Horizontal Dilution of Precision

A GNSS receiver's positional fix inaccuracy caused by the geometry of the navigational satellites from which signals are received is referred to as "dilution of precision" (DOP). The number of satellites that are visible (for line-of-sight propagation), their altitude, and the bearing towards them are referred to as geometry in the term geometric dilution of precision (GDOP). DOP may be thought of as the ratio of position error to range error and is just a value of probability for the geometrical influence on GPS accuracy. The geometric correlations between the receiver location and the positions of the navigational satellites are employed to calculate the DOP in its entirety, which may be a complicated process. For a full positional fix in three dimensions, a GNSS receiver typically only needs four satellite signals. The exact locations of the four satellites concerning the receiver affect this fix's accuracy to some extent. The fix will be quite accurate if the four signals are from satellites that are dispersed throughout the sky as seen from the receiver. The fix, however, will be less precise if all four satellites are near one another inside a single quadrant. A fix might not be achievable if two or more satellites are lined up and appear to share the same space. The fix might also be inaccurate by as much as 150 or 200 meters. The geometry is considered to be weak, and the DOP value is high when the visible navigation satellites are close together in the sky; the geometry is said to be strong, and the DOP value is low when they are far apart. Considering the greater angular separation between the satellites required to determine a GNSS receiver unit's location, a low DOP value denotes a superior positional precision.

The term **"Horizontal DOP (HDOP)"** refers to the impact of DOP on the value of the horizontal position. The HDOP and horizontal position (Latitude and Longitude) are better the more good visible satellites there are low in the sky.[24]

The GPS accuracy is expressed by the formula,

$$\sigma_p = DOP.\sigma_{UERE}, \tag{2.9}$$

Where, σ_p is standard deviation of position accuracy.c

σ_{UERE} is standard deviation of satellite pseudorange measurement error

DOP is dilution of precision which could be HDOP, VDOP, PDOP, and so forth.

2.3. Fusion Algorithms

In this chapter, we will review the basic concepts of sensor fusion, especially the methods that will be used in this work. Sensor fusion can help combine information

from several sensors resulting in better performing information in most cases. It can also combine information from complementary sensors that individually obtain part of the necessary information. The equation (2.10) describes a linear sensor model.

$$y_k = H_k x + e_{k,} \qquad k = 1, \dots, N \tag{2.10}$$

Where $y_1, \dots, y_N$ are the N available sensor measurements and x is the unknown state to be estimated, e_k is the sensor noise which usually is unknown. The k index lists the sensor readings and might correspond to a time index.

A simplified notation of sensor equation is shown in equation (2.11) where the vector $\mathbf{y}$ contains all sensor measurements y_k and likewise for H_k and e_k .

$$\boldsymbol{y} = \boldsymbol{H}x + \boldsymbol{e}. \tag{2.11}$$

2.3.1. Least-square Method

The optimization problem represented by equations (2.12) and (2.13) has as solution the least squares (LS) estimate.

$$\hat{x}^{LS} = \arg\min_x V^{LS}(x) \tag{2.12}$$

$$\begin{aligned} V^{LS}(x) &= \sum_{k=1}^{N} (y_k - H_k x)^T (y_k - H_k x) \\ &= (\mathbf{y} - \mathbf{H}\mathrm{x})^{\mathrm{T}} (\mathbf{y} - \mathbf{H}\mathrm{x}), \end{aligned} \tag{2.13}$$

$V^{LS}(x)$ is the quadratic loss function, and $\underset{x}{argmin}$ means the minimizing argument. Equation (2.14) is the result of solving the quadratic optimization problem and the estimate is $\hat{x}^{LS}$.

$$\hat{x}^{LS} = \left(\sum_{k=1}^{N} {H_k}^T H_k\right)^{-1} \sum_{k=1}^{N} {H_k}^T y_k = (\mathbf{H}^{\mathrm{T}}\mathbf{H})^{-1}\mathbf{H}^{\mathrm{T}}\mathbf{y}. \tag{2.14}$$

2.3.2. Weighted Least-square Method

If the information of the covariance of the measurement errors is accessible and we know that $\mathrm{Cov}(e_k) = R_k$ and $\mathbf{R} = \mathrm{diag}(R_1 \ldots . R_N)$, then Weighted Leas Square (WLS) is a better option to estimate the system state. The WLS estimate is found by minimizing the following loss function

$$\hat{x}^{WLS} = \arg\min_x V^{WLS}(x), \tag{2.15}$$

$$V^{WLS}(x) = \sum_{k=1}^{N}(y_k - H_k x)^T R_k^{-1}(y_k - H_k x)^T R_k^{-1} = (\mathbf{y} - \mathbf{H}\mathrm{x})^{\mathrm{T}}\mathbf{R}^{-1}(\mathbf{y} - \mathbf{H}\mathrm{x}). \tag{2.16}$$

The estimate solution is given by equation (2.17).

$$\begin{aligned}\hat{x}^{WLS} &= \left(\sum_{k=1}^{N} H_k{}^T R_k^{-1} H_k\right)^{-1} \sum_{k=1}^{N} H_k{}^T R_k^{-1} y_k \\ &= (\mathbf{H}^{\mathrm{T}}\mathbf{R}^{-1}\mathbf{H})^{-1}\mathbf{H}^{\mathrm{T}}\mathbf{R}^{-1}\mathbf{y}.\end{aligned} \tag{2.17}$$

WLS is known as the *best linear unbiased estimator (BLUE)* of x even though the noise is non-gaussian, but it should have zero mean.

2.3.3. Kalman Filter Method

Sensor fusion for dynamic systems requires dynamic models and information available from measurement y_k to estimate an unkwon system state x_{k+1} where k represent a time indicator. A linear state space model is represented by the following equations:

$$x_{k+1} = F_k x_k + B_k u_k + w_k,\ \mathrm{Cov}(w_k) = Q_k. \tag{2.18}$$

$$y_k = H_k x_k + e_k, \qquad \mathrm{Cov}(e_k) = R_{k.}$$

$$E(x_1) = \hat{x}_{1|0}. \qquad \mathrm{Cov}(x_1) = P_{1|0}.$$

The state matrix $x \in \mathbb{R}^n$ at time $t = t_k$ is defined as x_k. Matrix $F_k \in \mathbb{R}^{n\times n}$ transforms linearly the state x_k to x_{k+1}. The vector w is known as noise process and it is assumed to be zero mean multivariate Gaussian distributed with covariance Q.

$u \in \mathbb{R}^l$ is known as control input and it represents environmental factors which are not represented in the model. $B \in \mathbb{R}^{n\times l}$ is a linear transformation matrix that converts control space into state space.

$y_k \in \mathbb{R}^m$ is the measurement with error e_k at time $t = t_k$. The error e_k is assumed to have Gaussian distributtion with zero mean and covariance R. $H \in \mathbb{R}^{m\times n}$ is a matrix that makes the linear transformation between state space and measurement space.

It has become clear that there are errors in the state estimates and in the measurements. We can obtain the best state estimate based on the information on the covariances of the state estimate and the measurement error, the best state estimate will be closer to the state estimate if its covariance is smaller than the error covariance of the measurement, on the other hand, if the covariance of the error measurement is smaller than the covariance of the state estimate, the best estimate will be closer to the measurement. We can use the Kalman filter equations to get the best state estimate.

Kalman filter has two steps: prediction, and update. In the prediction part, the system model is used to calculate the predicted state estimate $\hat{x}_{k+1|k}$, this is also called a priori estimate since it is calculated before the current measurement is taken, and the error covariance $P_{k+1|k}$. Equation (2.25) shows that $P_{k+1|k}$ is calculated from the process noise Q_k and the error covariance $P_{k|k}$. At the beginning of the algorithm, the initial estimates $\hat{x}_{1|0}$ and $P_{1|0}$ are used to calculate the a priori estimate and its error covariance.

The Update step of the algorithm uses the a priori estimates calculated by equations (2.24) and (2.25) and updates them in equation (2.20) and (2.21) to find the posteriori estimates $\hat{x}_{k|k}$ and error covariance $P_{k|k}$. Equation (2.9) calculates the Kalman gain in a way that minimizes the a posterior error covariance $P_{k|k}$.

Measurement update:

Innovation (measurement residual)	$\epsilon_k = y_k - H_k \hat{x}_{k\|k-1}$	(2.19)
Innovation covariance	$S_k = H_k P_{k\|k-1} {H_k}^T + R_k$	(2.20)
Kalman Gain	$K_k = P_{k\|k-1} {H_k}^T {S_k}^{-1}$	(2.21)
Updated state estimate	$\hat{x}_{k\|k} = \hat{x}_{k\|k-1} + K_k \epsilon_k$	(2.22)
Updated estimate covariance	$P_{k\|k} = (I - K_k H_k) P_{k\|k-1}$	(2.23)

Prediction update:

Predicted state estimate	$\hat{x}_{k+1\|k} = F_k \hat{x}_{k\|k} + B_k u_k$	(2.24)
Predicted estimate covariance	$P_{k+1\|k} = F_k P_{k\|k} {F_k}^T + Q_k$	(2.25)

The Kalman gain determines how much the measurement y_k and the a priori estimate $\hat{x}_{k|k-1}$ contribute to the calculation of $\hat{x}_{k|k}$. if the measurement noise is small the measurement contributes more to the calculation of $\hat{x}_{k|k}$ than the a priori state estimate. On the other hand, when the error of the a priori estimate is small, the calculation of $\hat{x}_{k|k}$ mostly comes from this estimate.

Once we calculate the updated equations, in the next step, the a posteriori estimates are used to predict the new a priori estimates, and the algorithm repeats.[32]

2.4 Motion Model

There are different motion models such as Constant Velocity (CV), Constant Acceleration (CA), Constant Turn (CT), etc. The CV model can be used to describe pedestrian movements and as a system model in the Kalman Filter algorithm [1]. Equation (2.26) shows the constant motion equation for a target moving at a constant velocity from time $k-1$ to time k[31].

$$\begin{aligned} x_k &= x_{k-1} + \Delta T \dot{x}_{k-1} \\ \ddot{x}_{k-1} &= 0 \end{aligned} \tag{2.26}$$

Where x_k and x_{k-1} are the positions at time k and $k-1$ respectively, ΔT is the sampling period, and $\dot{x}_{k-1}$ is the velocity at time $k-1$ and $\ddot{x}_{k-1}$ is acceleration.

To have a more accurate description of the movement, equation (2.27) includes an acceleration to calculate the position of a target, where $\ddot{x}_{k-1} = w_{x,k-1}$.

$$x_k = x_{k-1} + \Delta T \dot{x}_{k-1} + \frac{\Delta T^2}{2} w_{x,k-1} \tag{2.27}$$

This acceleration can be defined as a zero-mean Gaussian noise as in equation (2.8).

$$w_{x,k-1} = \ddot{x}_{k-1} \sim \mathcal{N}(0, \sigma^2_{x,k-1}) \tag{2.28}$$

Where, $\sigma^2_{x,k-1}$ is the variance that determines the degree of change in the velocity in the constant velocity model. Equation (2.29) shows how the state of the target changes while it moves from time $k-1$ to k, where $w_{x,k-1}$, $w_{y,k-1}$are the process noises of x_k, y_k respectively.

$$\begin{aligned} x_k &= x_{k-1} + \Delta T \dot{x}_{k-1} + \frac{\Delta T^2}{2} w_{x,k-1} \\ y_k &= y_{k-1} + \Delta T \dot{y}_{k-1} + \frac{\Delta T^2}{2} w_{y,k-1} \\ \dot{x}_k &= \dot{x}_{k-1} + \Delta T w_{x,k-1} \\ \dot{y}_k &= \dot{y}_{k-1} + \Delta T w_{y,k-1} \end{aligned} \tag{2.29}$$

Equation (2.30) represents equation (2.29) in matrix form.

$$\begin{bmatrix} x_k \\ y_k \\ \dot{x}_k \\ \dot{y}_k \end{bmatrix} = \begin{bmatrix} 1 & 0 & \Delta T & 0 \\ 0 & 1 & 0 & \Delta T \\ 0 & 0 & 1 & 0 \\ 0 & 0 & 0 & 1 \end{bmatrix} \begin{bmatrix} x_{k-1} \\ y_{k-1} \\ \dot{x}_{k-1} \\ \dot{y}_{k-1} \end{bmatrix} + \begin{bmatrix} \frac{\Delta T^2}{2} w_{x,k-1} \\ \frac{\Delta T^2}{2} w_{y,k-1} \\ \Delta T w_{x,k-1} \\ \Delta T w_{y,k-1} \end{bmatrix} \tag{2.30}$$

Equation (2.30) can also be represented as,

$$\mathbf{X_k} = \mathbf{F_{k-1}} \mathbf{X_{k-1}} + \mathbf{W_{k-1}}. \tag{2.31}$$

Where the values of $\mathbf{F_{k-1}}$ can be found in the equation (2.30) and $\mathbf{W_{k-1}} \sim \mathcal{N}(0, Q_{k-1})$. The process noise covariance $\mathbf{Q_{k-1}}$ is calculated using the covariance of $\boldsymbol{W_{k-1}}$ as shown in the equation (2.32).

$$\mathbf{Q_{k-1}} = Cov(\mathbf{W_{k-1}}) = E[\mathbf{W_{k-1}} \mathbf{W^T}_{\mathbf{k-1}}] \tag{2.32}$$

Where, $E[W_{k-1} {W^T}_{k-1}]$ is expected value of $W_{k-1} {W^T}_{k-1}$. Q_{k-1} can be calculated as follow

$$\boldsymbol{Q_{k-1}}$$

$$= E\left[\begin{bmatrix}\frac{\Delta T^2}{2}w_{x,k-1}\\ \frac{\Delta T^2}{2}w_{y,k-1}\\ \Delta T w_{x,k-1}\\ \Delta T w_{y,k-1}\end{bmatrix}\begin{bmatrix}\frac{\Delta T^2}{2}w_{x,k-1} & \frac{\Delta T^2}{2}w_{y,k-1} & \Delta T w_{x,k-1} & \Delta T w_{y,k-1}\end{bmatrix}\right]$$

$$= \begin{bmatrix}\frac{\Delta T^4}{4}\sigma_{w_x}^2 & 0 & \frac{\Delta T^3}{2}\sigma_{w_x}^2 & 0\\ 0 & \frac{\Delta T^4}{4}\sigma_{w_y}^2 & 0 & \frac{\Delta T^3}{2}\sigma_{w_y}^2\\ \frac{\Delta T^3}{2}\sigma_{w_x}^2 & 0 & \Delta T^2\sigma_{w_x}^2 & 0\\ 0 & \frac{\Delta T^3}{2}\sigma_{w_y}^2 & 0 & \Delta T^2\sigma_{w_y}^2\end{bmatrix}, \quad (2.33)$$

Where $\sigma_{w_x}^2$ and $\sigma_{w_y}^2$ are the variance of the process noise in each coordinate.

The equation 2.35 models the measurent $\mathbf{Z_k}$ as a noisy version of the system state $\mathbf{X_k}$. In equation (2.34), the matrix version of the measurent model is calculated where $v_{x,k}$, $v_{y,k}$, $v_{\dot{x},k}$and $v_{\dot{y},k}$ are observation noises corresponding to $z_{x,k}$, $z_{y,k}$, $\dot{z}_{x,k}$ and $\dot{z}_{y,k}$, respectively, which are basically zero-mean Gaussian white noises.

$$\boldsymbol{Z_k = H_k X_k + V_k} \quad (2.34)$$

$$\begin{bmatrix}z_{x,k}\\ z_{y,k}\\ \dot{z}_{x,k}\\ \dot{z}_{y,k}\end{bmatrix} = \begin{bmatrix}1 & 0 & 0 & 0\\ 0 & 1 & 0 & 0\\ 0 & 0 & 1 & 0\\ 0 & 0 & 0 & 1\end{bmatrix}\begin{bmatrix}x_k\\ y_k\\ \dot{x}_k\\ \dot{y}_k\end{bmatrix} + \begin{bmatrix}v_{x,k}\\ v_{y,k}\\ v_{\dot{x},k}\\ v_{\dot{y},k}\end{bmatrix} \quad (2.35)$$

In equation (2.34), $V_k \sim \mathcal{N}(0, R_k)$, the value of R_k can be obtained by taking the covariance of V_k as

$$R_k = Cov(V_k) = E[V_k {V^T}_k] \quad (2.36)$$

Now, R_k can be given as

$$R_k = E\left[\begin{bmatrix}v_{x,k}\\ v_{y,k}\\ v_{\dot{x},k}\\ v_{\dot{y},k}\end{bmatrix}\begin{bmatrix}v_{x,k} & v_{y,k} & v_{\dot{x},k} & v_{\dot{y},k}\end{bmatrix}\right] = \begin{bmatrix}\sigma_{v_x}^2 & 0 & 0 & 0\\ 0 & \sigma_{v_y}^2 & 0 & 0\\ 0 & 0 & \sigma_{v_{\dot{x}}}^2 & 0\\ 0 & 0 & 0 & \sigma_{v_{\dot{y}}}^2\end{bmatrix} \quad (2.37)$$

Chapter 3

Measurement and Data Acquisition

3.1. Bluetooth data acquisition

To get BLE positioning data, devices of the u-Blox company were used. Figure 3.1 shows how the BLE and GNSS data are obtained using XPLR-IOT-1. In this section a brief description of the hardware is done and how the BLE position estimation is calculated.

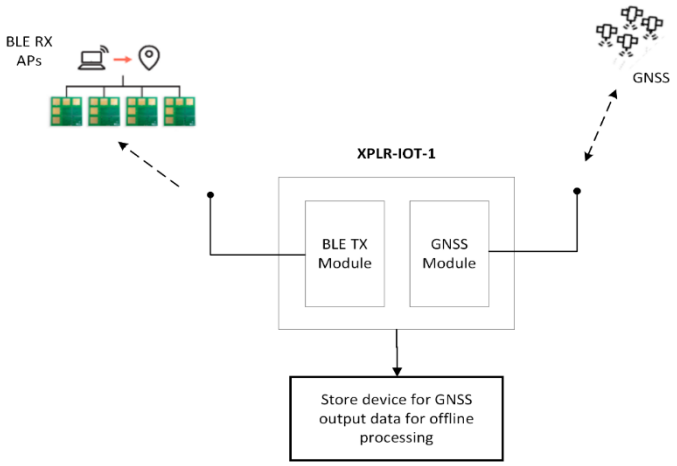

Figure 3.1: XPLR-IOT-1 device is used to obtain BLE and GNSS position estimation in the same environment [26].

3.1.1. Hardware

XPLR-IOT-1:

A full framework for creating multiple proof-of-concept IoT applications is offered by the XPLR-IOT-1 explorer kit. Wi-Fi, Bluetooth, and LTE-M/NB-IoT cellular connectivity are all supported by the gadget. Accurate positional information is provided by a specialized low-power GNSS receiver. Temperature, humidity, pressure, ambient light, a magnetometer, a gyroscope, an accelerometer, and a battery indicator are all included within the device.

Application software that is pre-flashed in the XPLR-IOT-1 kit is also available as source code. For publishing to the Thingstream platform, where the Data Flow

Manager receives and analyses the data, it gathers sensor and positional data from the device. Figure 3.2 is the XPLR-IOT-1 device[26].

Figure 3.2: Device XPLR-IOT- **[26]**

Communication and positioning features:

Cellular: SARA-R510S: LTE-M, and NB-IoT
Wi-Fi: NINA-W156: Wi-Fi 4, 2.4 GHz
Bluetooth: NORA-B106: v5.2 Low Energy
Satellite positioning: MAX-M10S: BeiDou, Galileo, GLONASS, and GPS

NINA-W15 series:

NINA-W15 series stand-alone multiradio modules integrate Wi-Fi, Bluetooth BR/EDR, and Bluetooth low energy in a compact form factor. The modules allow for simultaneous Bluetooth and Wi-Fi operation and can therefore act as a gateway between Bluetooth and Ethernet or Wi-Fi. The pre-flashed application software for the NINA-W15 modules supports dual-mode Bluetooth (Bluetooth BR/EDR v4.2+EDR and Bluetooth Low Energy v4.2) in the 2.4 GHz ISM band and Wi-Fi 802.11b/g/n. Through the AT command interface, the host system may configure and manage the module. Telematics, industrial automation, linked buildings, wireless sensors, point-of-sale systems, and medical equipment are just a few of the intended uses[27].

NINA-B411 , B41 series:

Stand-alone Bluetooth 5.1 low energy modules
Bluetooth 5.1 module for harsh professional environments [28].

- Bluetooth 5.1 module with long range and direction finding support
- u-connect software for accelerated time to market
- Extended temperature range to 105 °C
- Superior security functionality
- Pin compatible with other NINA modules
- Global certification

Anchor points:

The BLE anchor points (AP), consist of an eight-element antenna array of the manufacturer u-Blox called ANT-B10, see Figure 3.3. The ANT-B10 is designed for BLE AoA direction finding systems. It measures the angle of an incoming BLE radio signal. With more than one ANT-B10 and using a position engine software the estimated position of the BLE device can be calculated in an indoor environment [29].

Figure 3.3: Antenna ANT-B10.

Patch antenna:

A narrowband, wide-beam antenna is a patch antenna or microstrip antenna. Additionally known as a printed antenna. It has physical geometry in two dimensions. A patch that is one-half wavelength long is used in the simplest patch antenna, which causes the metal surface to resonate like a half-wave dipole antenna. A patch antenna is often made by bonding a continuous metal layer to the opposite side of the substrate, which serves as the ground plane and putting a shaped metal sheet on an insulating dielectric substrate, such as a printed circuit board. As a result, it is simple to design and cheap to produce. Some patch antennas

are built of a metal patch positioned atop a ground plane utilizing dielectric spacers rather than a dielectric substrate. The resultant structure has a broader bandwidth but is less robust. Patch antennas may be created for frequencies ranging from the UHF band to 100 GHz[30]. A microstrip or patch antenna has a wide radiating pattern. Its frequency bandwidth is constrained, and its radiation power is limited. Below is a diagram illustrating the radiation pattern of a microstrip or patch antenna. The diversity of the Patch antenna is weak. Radiation pattern is shown in figure 3.4.

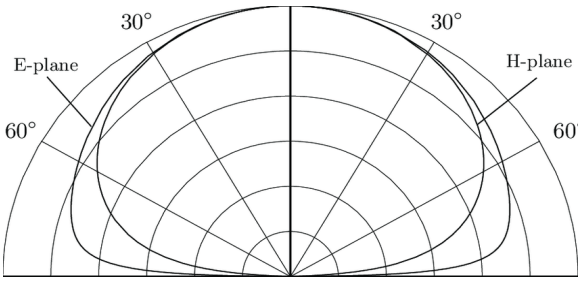

Figure 3.4: Radiation pattern of a Patch antenna **[30]**

3.1.2. Data Obtained from BLE

To get reliable BLE measurements several APs were used in the tests. These APs receive the beacon from the BLE tag which contains IQ samples, the APs use this IQ information to calculate the AoA using estimator algorithms such as MUSIC or PDDA. Then the data of each AP is introduced to the Position Engine to calculate the estimate position of the tag using a Least Square algorithm.

The rate that BLE position engine estimates a tag position is around 25 positions per second. This is an important parameter because we will use it to calculate the covariance matrix of the measurements which is used in the fusion algorithms later, besides the final position also the other information can be obtained from this equipment such as RSSI, the time when a packet is received by each anchor point among others. Figure 3.5 shows a diagram flow of how the position of a BLE tag is estimated.

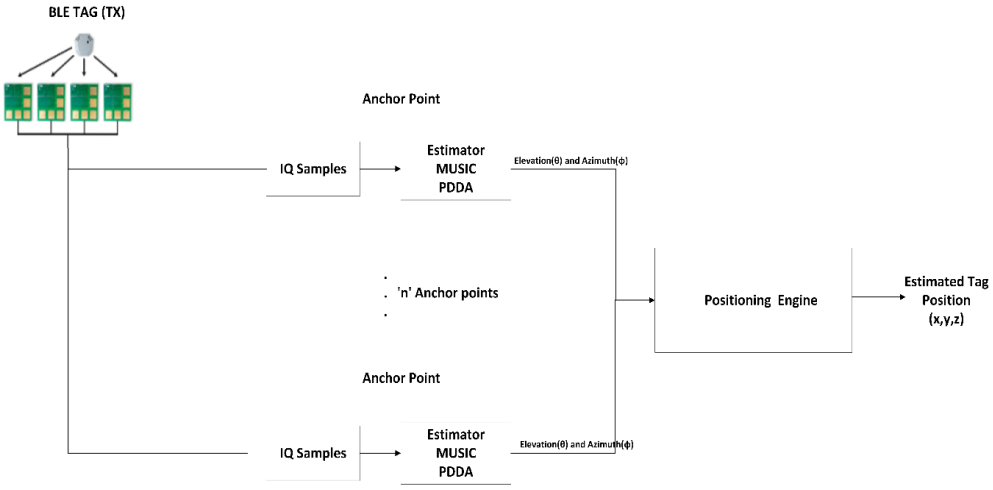

Figure 3.5: Position estimation flow using BLE technology **[26].**

3.2. GNSS Data Acquisition

In this section, we will discuss how we get the simulated GNSS data by providing the ground truth (GT) to the simulator and also the GNSS real data readings with the help of the XPLT-IOT-1 device. Later in Chapter 6, we will compare these results and analyze the difference.

3.2.1. GNSS Real data acquisition

In this section, we will discuss about how we obtained the real GNSS position values. We will talk about 3 scenarios, i.e., Indoor, Indoor – Outdoor and Outdoor.

Indoor real data acquisition

Here were are using both the technologies BLE as well as GNSS. Most of the positioning data obtained in this scenario are mostly from the BLE anchor points, the anchor points are placed as shown in the figure 3.1. We are also making use of the XPLR-IOT-1 device, as the measurement is taken near the window and keeping in mind there might be some visible satellites. Due to shadowing and different obstacles we only received a few GNSS packets while most of the values were got from the BLE.

Indoor – Outdoor real data acquisition

This scenario is where we will apply a fusion algorithm to make the indoor-outdoor positioning more accurate. Here, for every one second we receive one packet of GNSS data but many Bluetooth data is received for every one second, hence every one packet of GNSS data will contain many packets of Bluetooth data. So, when

we're outdoor there is no BLE data obtained, we have to match the point where we are receiving data from both technologies.

Outdoor real data acquisition

In this case, we completely used the XPLR-IOT-1 device to obtain the data. During the measurement, there are a few factors considered like shadowing, the velocity at which we walk, and the standard height of a person. There are no Bluetooth data considered here since they are used for an indoor purpose and also for indoor-outdoor fusion.

3.3. Measurement setup

Indoor measurement setup:

For our indoor measurements, we have considered the U-blox office, which is on the 5th floor of the building. The below figure 3.1 shows the outline prototype of our measurement setup, where the blue dots indicates the placements of our BLE anchor points and the red line shows the path trajectory in which we have taken our readings.

In figure 3.6, we can see the actual indoor environment. Here, throughout our measurement trajectory, we have a large glass window that gives us some readings from the GNSS along with the BLE readings. But still, we will come across some amount of shadowing due to other buildings and since it's indoor. Thus the GNSS values received will not be strong enough compared with the BLE values.

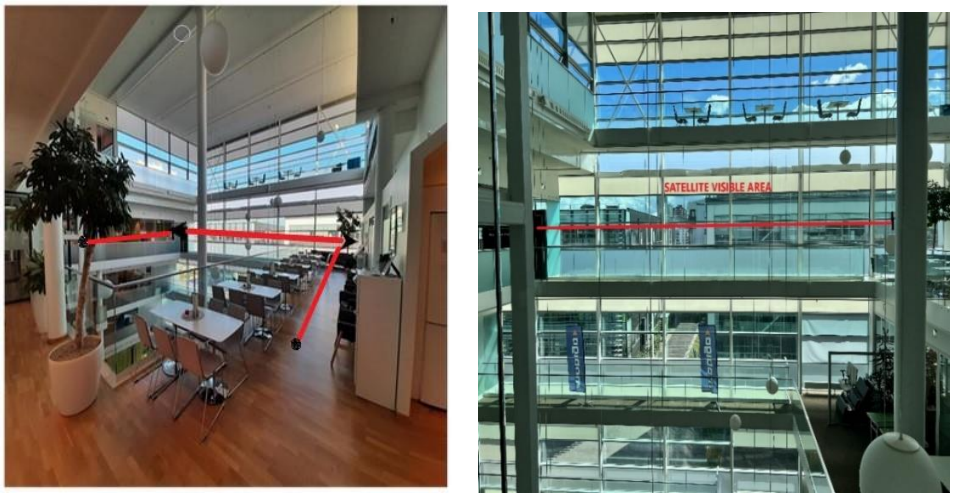

Figure 3.6: Indoor measurement setup

Outdoor measurement setup:

Figure 3.7 shows the outdoor measurement outline. The outdoor measurement was taken around the U-blox building with the help of the XPLR-IOT-1 device. In this setup, we are only considering the GNSS received data and not the BLE since we are using the BLE only for indoor measurements.

Figure 3.7: Outdoor measurement scenario

Indoor – Outdoor Scenario:

In this case, the anchor points are placed inside the building to get the measurements from BLE and with the help of XPLR-IOT-1, we are collecting the GNSS data once we start moving out of the building. The device will start to capture GNSS data once there is a transition from indoor to outdoor i.e., near the entrance. And once we are outdoor we will only capture the GNSS readings. Since there is a transition from indoor to outdoor and also there due to buildings outdoor, received data will have shadowing. The path trajectory of the indoor-outdoor scenario is shown in figure 3.8. and figure 3.9. The red line is the trajectory traced.

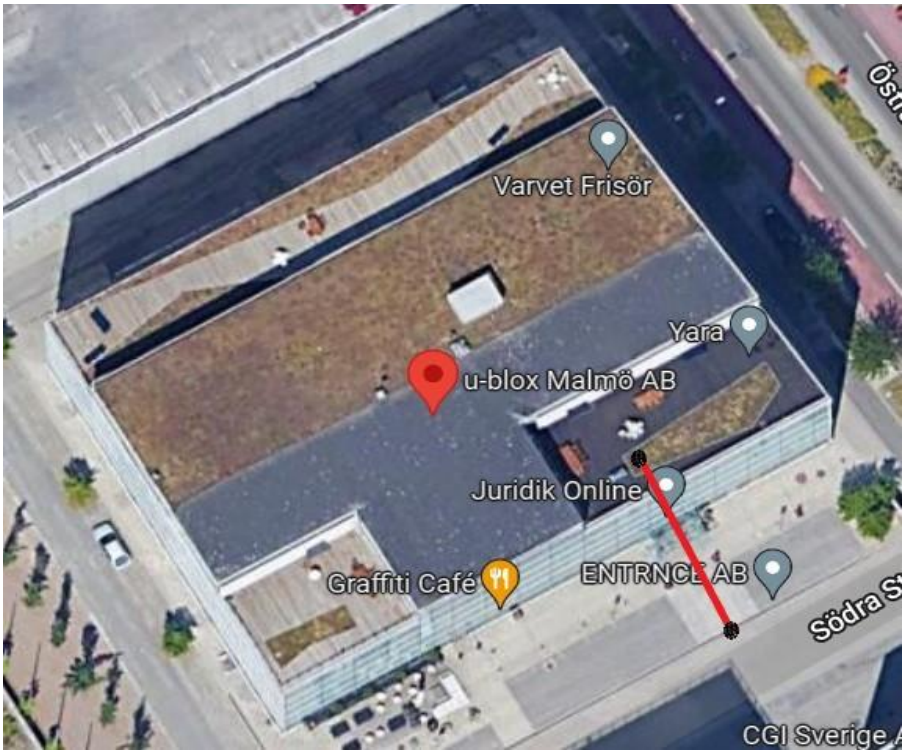

Figure 3.8: Indoor – Outdoor measurement path1

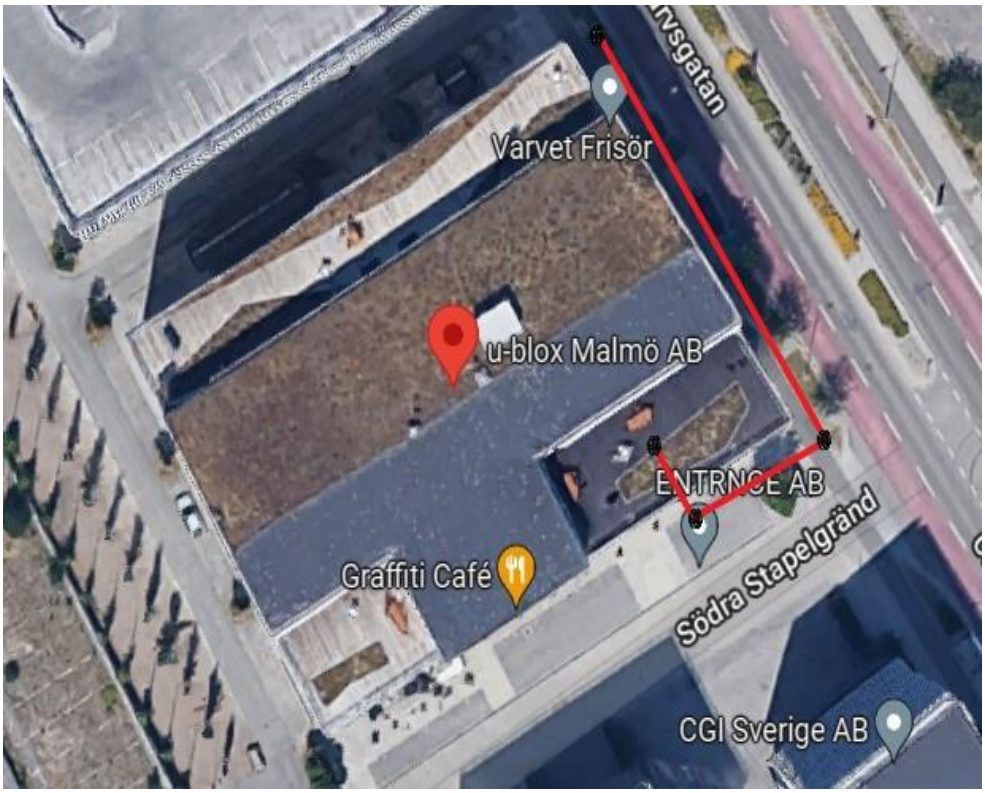

Figure 3.9: Indoor – Outdoor measurement path2

Indoor setup of Anchor Points:

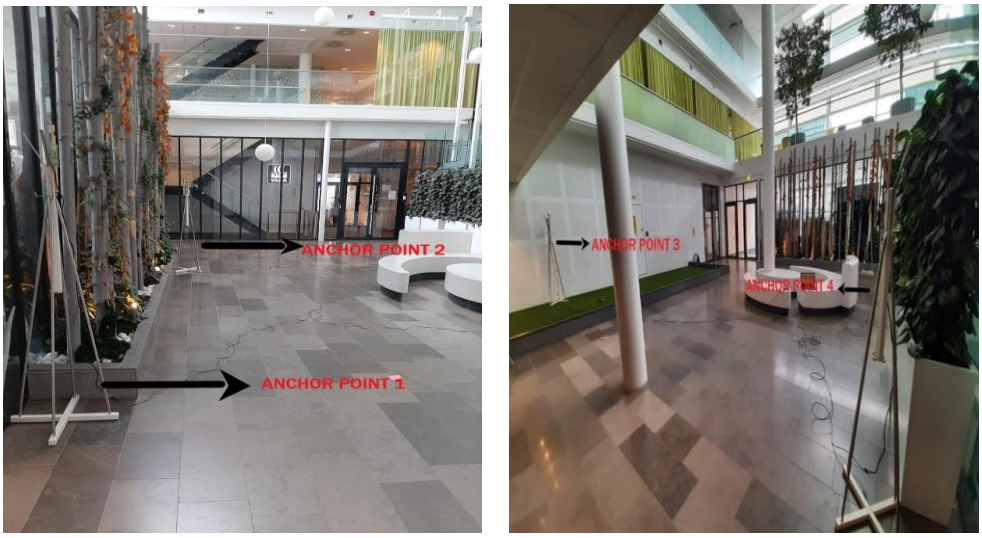

(a) **(b)**

Figure 3.10 (a)&(b): Placements of anchor points inside the building

3.4. Hybrid fusion

3.4.1. Weighted Least Square Fusion

Using the formula (2.11) for the sensor model we can model the measurement received from BLE and GNSS, since we are trying to merge two position information to estimate another position it means that there is no need for any transformation hence, we will consider $\mathbf{H} = \mathbf{I}$ in equation (2.17).

To apply WLS, information about error covariance is needed, for BLE estimates, it is obtained by equation (3.2), where σ_{BLE} is the standard deviation of the error of all the BLE measurements taken in the tests. The covariance matrix of GNSS measurements is calculated using equation (3.4), where σ_p is the standard deviation of the error of the estimated position for GPS, to calculate σ_p, HDOP and the pseudorange error budged for GPS Standard Position Service are used according to the equation (2.9).

The measurement position estimates for BLE and GNSS are represented in equations (3.1) and (3.3) respectively.

$$\boldsymbol{y_{BLE} = x + e_{BLE},} \tag{3.1}$$

$$Cov(e_{BLE}) = \mathbf{R_{BLE}} = {\sigma_{BLE}}^2 \mathbf{I}_2 \,. \tag{3.2}$$

$$\boldsymbol{y_{GNSS}} = \boldsymbol{x} + \boldsymbol{e_{GNSS}}, \tag{3.3}$$

$$Cov(e_{GNSS}) = \mathbf{R_{GNSS}} = \ {\sigma_p}^2 \mathbf{I}_2 \,. \tag{3.4}$$

The fusion algorithm using WLS is shown in equation (3.5)

$$\hat{\mathbf{x}} = \left(\mathbf{R_{BLE}^{-1}} + \mathbf{R_{GNSS}^{-1}}\right)^{-1}\left(\mathbf{R_{BLE}^{-1}}\mathbf{y_{BLE}} + \mathbf{R_{GNSS}^{-1}}\mathbf{y_{GNSS}}\right). \tag{3.5}$$

The position estimate by WLS is $\hat{\mathbf{x}} = \ [\hat{x} \quad \hat{y}]^T$, where $\hat{x}$ and $\hat{y}$ are the estimates location coordinates.

3.4.2. Kalman Filter Fusion

To merge the position estimates received from BLE and GNSS using Kalman filter, first, we will define the measurement vector $\boldsymbol{y_k}$ used in equation (2.17). This vector is composed of the measurements received from BLE and GNSS and it is shown in equation (3.7). The measurement vectors of position estimates from BLE and GNSS include the coordinates of the position estimation given by each technology (equation (3.6)).

$$\mathbf{y_{GNSS}} = \begin{bmatrix} x_{GNSS} \\ y_{GNSS} \end{bmatrix};\ \mathbf{y_{BLE}} = \begin{bmatrix} x_{BLE} \\ y_{BLE} \end{bmatrix} \tag{3.6}$$

$$\boldsymbol{y_k} = \begin{bmatrix} \boldsymbol{y_{GNSS}} \\ \boldsymbol{y_{BLE}} \end{bmatrix}. \tag{3.7}$$

The matrix $\mathbf{H_k}$ for the fusion process is shown in equation (3.6), In this work this transformation matrix will not change through time.

$$\mathbf{H_k} = \begin{bmatrix} \mathbf{I}_4 \\ \mathbf{I}_4 \end{bmatrix}; \tag{3.8}$$

The covariance matrix $\mathbf{R_k}$ that is used in equation (2.18) includes the covariance of GNSS measurements $\mathbf{R_{GNSS}}$ and the covariance of BLE measurements $\mathbf{R_{BLE}}$ as they are calculated in equation (3.2) and (3.4).

$$\mathbf{R_k} = \begin{bmatrix} \mathbf{R_{GNSS}} & \mathbf{0} \\ \mathbf{0} & \mathbf{R_{BLE}} \end{bmatrix}. \tag{3.9}$$

The model derived in section 2.4 is used as system model in this work, therefore the terms of the equations in the prediction part of Kalman filter algorithm have the same form of the equations of the motion model (2.31). $\mathbf{B_k u_k = 0}$ in equation (2.24) and $\mathbf{Q_k}$ is calculated using the equation (2.25), where $\sigma_{w_x}^2$ and $\sigma_{w_y}^2$ are derivate from the standard deviation of the velocity variation in x and y coordinates respectively. After replacing the terms in the equation (2.24) we have:

$$\begin{bmatrix} \hat{x}_{k+1|k} \\ \hat{y}_{k+1|k} \\ \dot{x}_{k+1|k} \\ \dot{y}_{k+1|k} \end{bmatrix} = \begin{bmatrix} 1 & 0 & \Delta t & 0 \\ 0 & 1 & 0 & \Delta t \\ 0 & 0 & 1 & 0 \\ 0 & 0 & 0 & 1 \end{bmatrix} \begin{bmatrix} \hat{x}_{k|k} \\ \hat{y}_{k|k} \\ \dot{x}_{k|k} \\ \dot{y}_{k|k} \end{bmatrix} + \mathbf{0} \tag{3.10}$$

Where:

$$\hat{\mathbf{x}}_{\mathbf{k+1|k}} = \begin{bmatrix} \hat{x}_{k+1|k} \\ \hat{y}_{k+1|k} \\ \dot{x}_{k+1|k} \\ \dot{y}_{k+1|k} \end{bmatrix}; \ \mathbf{F_k} = \begin{bmatrix} 1 & 0 & \Delta t & 0 \\ 0 & 1 & 0 & \Delta t \\ 0 & 0 & 1 & 0 \\ 0 & 0 & 0 & 1 \end{bmatrix}; \ \hat{\mathbf{x}}_{\mathbf{k|k}} = \begin{bmatrix} \hat{x}_{k|k} \\ \hat{y}_{k|k} \\ \dot{x}_{k|k} \\ \dot{y}_{k|k} \end{bmatrix} \tag{3.11}$$

The final state of our system $\hat{\mathbf{x}}_{\mathbf{k|k}}$ is calculated by replacing the results of equations (3.7), (3.8), and (3.11) in the equations of the update step of Kalman filter. In equation (2.20), $\hat{\mathbf{x}}_{\mathbf{k|k}}$ is the final state estimation of the fusion algorithm using Kalman filter.

Chapter 4

Results

4.1. Measurements and plots

4.1.1. Field Measurements & Fusion Results

As mentioned in chapter 3.4, measurements were made in three types of environments: indoor, indoor-outdoor, and outdoor. This section will show the results of the measurements made in each of these scenarios.

For the indoor test, the average absolute BLE position error was 2.53 m with a 90-percentile of 4.01 m. The average absolute GNSS position error was 10.98 m with a 90-percentile error of 18.57 m, while the average absolute WLS position error was 2.55 m and the 90-percentile for this fusion method was 4.01 m. The average position error of Kalman filter (KF) was 2.84 m, and the 90-percentile was 4.50 m. Figure 4.1 shows the average positioning output for all the technologies used. In Figure 4.2, the CDF, and 90-percentile of the errors for all the technologies are presented.

Below presented graphs is the output of average of all the indoor measurements taken.

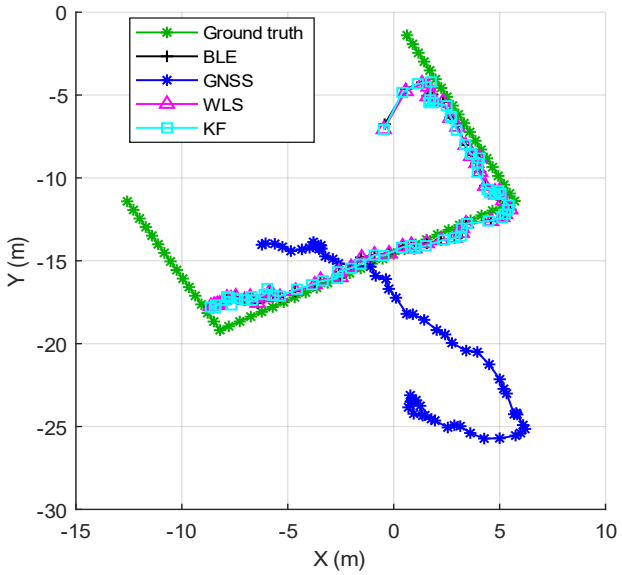

Figure 4.1. Ground Truth, BLE, GNSS, WLS, and KF outputs for indoor test.

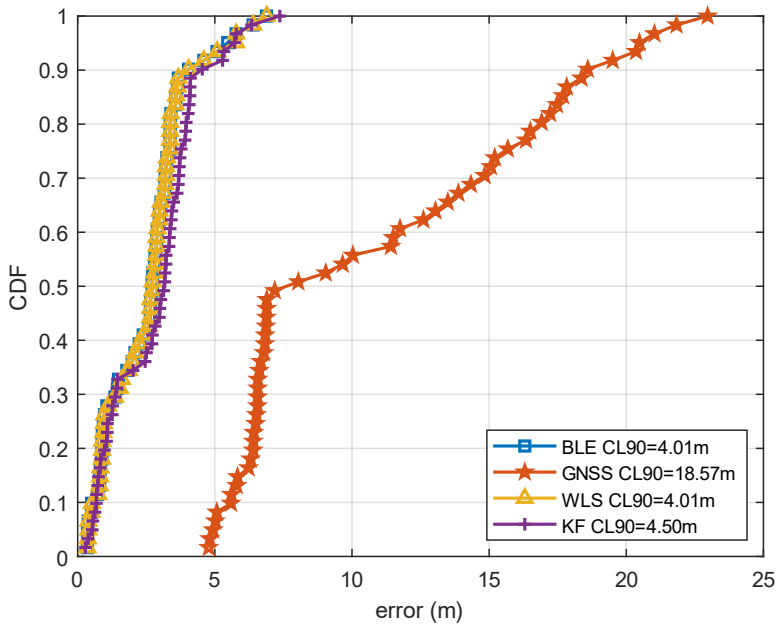

Figure 4.2. Cumulative distribution function of position error for indoor test.

Figure 4.3 (a) &(b) shows the average trajectories that were followed in the indoor-outdoor tests. In indoor-outdoor test 1, the trajectory is a straight line (Figure 4.3 (a)), and the velocity of the tag is constant. Table 4.1 shows that the average error is 3.68 m when WLS was used and 2.94 m when KF was used for the fusion of the positions obtained from BLE and GNSS. These average errors are lower than those obtained by using only BLE or GNSS. On the other hand, in the indoor-outdoor 2 test, where the path includes changes of direction (Figure 4.3 (b)), the average error using WLS was 4.64 m, which is lower than the 4.81 m average error obtained by KF.

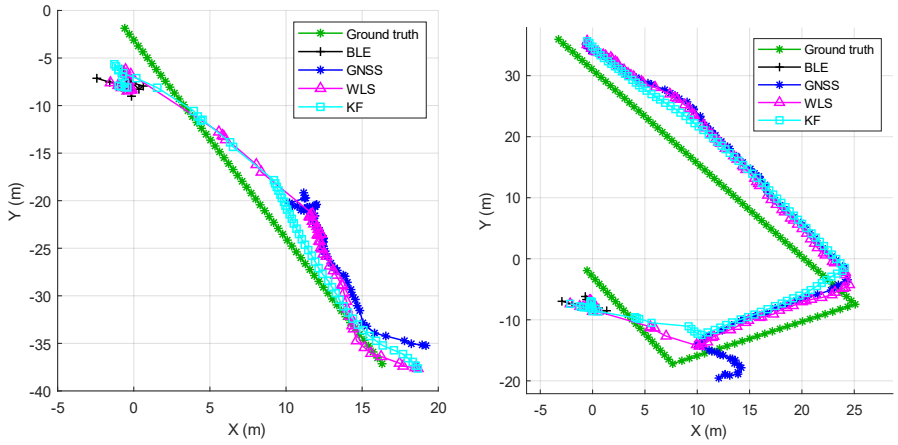

(a) **(b)**

Figure 4.3 (a) & (b) Ground Truth, BLE, GNSS, WLS, and KF outputs for indoor-outdoor test 1&2.

Figures 4.4 (a) & (b) present the CDF for the error of indoor-outdoor test 1 and indoor-outdoor test 2 respectively. For indoor-outdoor test 1, the 90-percentile error of WLS was 6.93 m, and 4.78 m for KF which are lower compared to the values obtained by BLE and GNSS. A similar result is obtained when we compare the 90 percentile errors of the indoor-outdoor test 2. WLS and KF have a lower 90 percentile error than BLE and GNSS (see Figure 4.4 (b)).

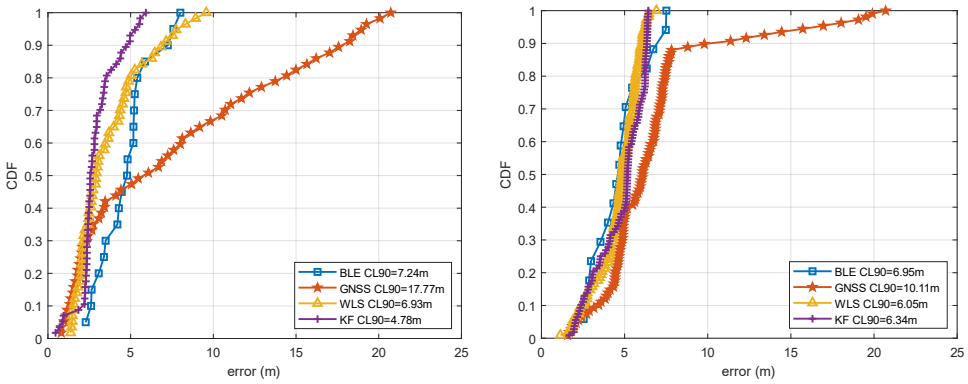

(a) **(b)**

Figure 4.4 (a) & (b). Cumulative distribution function of position error for indoor-outdoor test 1 & 2.

	Indoor Error	Indoor-outdoor test 1 Error	Indoor-outdoor test 2 Error	Outdoor Error
BLE	2.53	4.75	4.72	N/A
GNSS	10.98	7.7	6.71	5.91
WLS	2.55	3.68	4.64	5.91
KF	2.84	2.94	4.81	11.15

Table 4.1. Average error (in meters) for field tests.

Additionally, an outdoor test was carried out; in this case, during the development of the test, no BLE readings were received since the test was carried out entirely outside. Figure 4.5 shows the path as well as the average estimates of the position of each technology used for all the outdoor tests performed. From Table 4.1, the average error for WLS is the same as for GNSS which is 5.91 m, while the average error for KF is 11.15 m. The 90-percentile error values for GNSS, WLS, and KF are 7.43 m, 7.43 m, and 18.64 m, respectively.

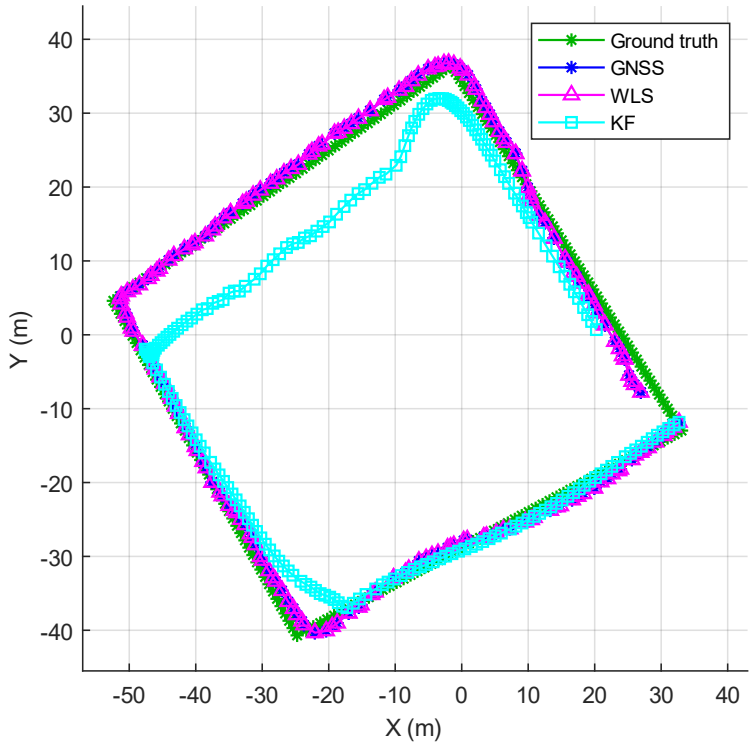

Figure 4.5. Ground Truth, BLE, GNSS, WLS, and KF outputs for outdoor test.

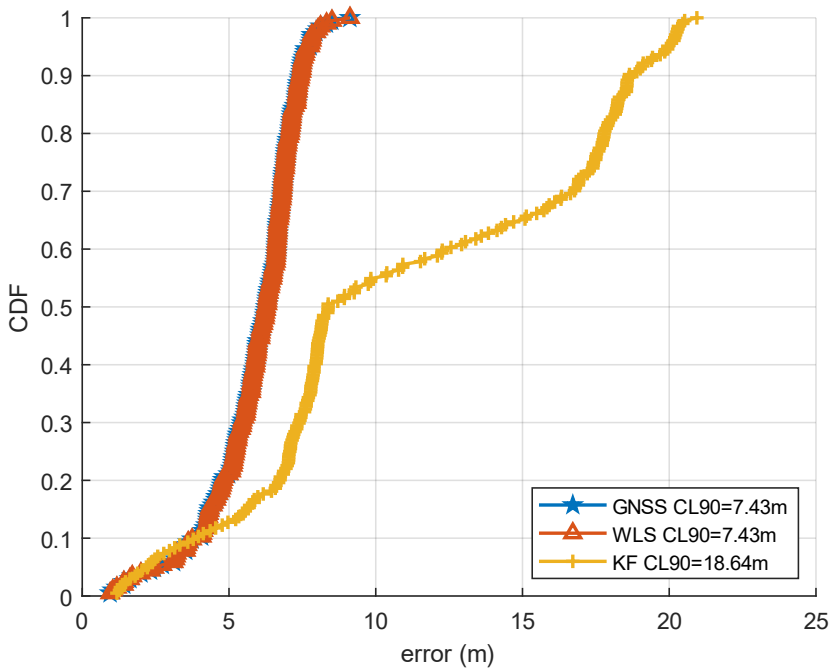

Figure 4.6. Cumulative distribution function of position error for outdoor test.

Chapter 5

Analysis

In Table 4.1, the error obtained using WLS is quite similar to the BLE error in the indoor test because the position estimates made by GNSS in this environment are not very exact, therefore WLS gives more weight to BLE position estimations. For the same test, the KF does not improve the accuracy compared with BLE but improves the accuracy by 74% compared with GNSS. The estimates of KF rely on the measurements and the prediction done by the model assumed since in our model we haven't included control information i.e., we consider $B_k u_k = 0$ in the prediction part of KF, even though we have considered a process noise in the model, it is necessary to have control information by time step to have more accurate results.

In the indoor-outdoor test 1. WLS and KF improve the accuracy compared to BLE by 23% and 38% respectively, they also have an improvement compared to GNSS which is 23% for WLS and 62% for the KF. In the indoor-outdoor test 2, we have a trajectory with sharp turns, under this condition WLS presents a slight improvement in the accuracy compared to BLE by 2% and almost 31% concerning GNSS, however, the performance of the KF is lower than using only BLE but improves the accuracy of GNSS by 28%. In the outdoor test, as only GNSS measurements are available the accuracy of WLS and GNSS are the same, on the other hand, the accuracy of KF is the lowest.

Chapter 6

Conclusion

In this thesis work, two Hybrid indoor-outdoor positioning systems (HPS) Weighted least square (WLS) and Kalman Filter (KF) are investigated. Both systems fuse positioning estimates obtained by Bluetooth Low Energy (BLE) AoA and GNSS technologies. In the investigated solutions, the fusion result is calculated by using the error accuracy given by the equipment used in the test. It is important to mention that the HPS based on the Kalman filter was designed by assuming a specific condition of a constant velocity of the target tag because the positioning devices used in the tests do not give information about acceleration. Several tests were carried on in indoor, indoor-outdoor, and outdoor environments. In all these tests, the performance of the HPSs proposed was as expected. The KF solution had a better performance in the environments where the velocity was constant in module and direction since in the system model considered, we haven't included information about control inputs, however, in the environments where the trajectory changes, the position accuracy did not improve when the KF was used. On the other hand, the solution based on WLS performed well in almost all the environments, except in the outdoors where its accuracy was equal to GNSS this is because the WLS solution does not depend on any model but on the standard deviation of the errors of each technology. In the indoor-outdoor environment, the proposed solution based on WLS improves the accuracy by up to 22% while the one based on KF enhances the accuracy by up to 38% compared to BLE performance, in the same environment the performance is improved compared with GNSS, HPS based on Kalman filter improves the accuracy up to 62% and HPS based in WLS improves the accuracy up to 31%. We conclude that the investigated HPSs improve the accuracy of the estimated position compared to BLE or GNSS in the indoor-outdoor environment.

6.1. Future Work

In this work, a constant velocity model was used for the solution based on KF without considering control input information which is very restrictive since it does not reflect the real behavior of the movement where it is affected by different factors such as the wind, driver maneuvers, etc. The use of a more general system is proposed as future work, to have more accurate estimations.

Perform the merger at an earlier stage of the position estimation process made by BLE and GNSS, to avoid the accumulation of errors due to intermediate processes in the calculation of the final position estimate.

References

[1] A. C. Eyng, O. K. Rayel, E. Oroski and J. L. Rebelatto, "Kalman Filtering-Aided Hybrid Indoor Positioning System With Fingerprinting And Multilateration," 2020 IEEE 91st Vehicular Technology Conference (VTC2020-Spring), 2020, pp. 1-5, doi: 10.1109/VTC2020-Spring48590.2020.9129422.

[2] R. Hansen, R. Wind, C. S. Jensen and B. Thomsen, "Seamless Indoor/Outdoor Positioning Handover for Location-Based Services in Streamspin," 2009 Tenth International Conference on Mobile Data Management: Systems, Services and Middleware, 2009, pp. 267-272, doi: 10.1109/MDM.2009.39.

[3] Z. Li, X. Zhao, F. Hu, Z. Zhao, J. L. Carrera Villacrés and T. Braun, "SoiCP: A Seamless Outdoor–Indoor Crowdsensing Positioning System," in IEEE Internet of Things Journal, vol. 6, no. 5, pp. 8626-8644, Oct. 2019, doi: 10.1109/JIOT.2019.2921561.

[4] Q. Lu, X. Liao, S. Xu and W. Zhu, "A hybrid indoor positioning algorithm based on WiFi fingerprinting and pedestrian dead reckoning," 2016 IEEE 27th Annual International Symposium on Personal, Indoor, and Mobile Radio Communications (PIMRC), 2016, pp. 1-6, doi: 10.1109/PIMRC.2016.7794982.

[5] J. A. Fernandez-Madrigal, E. Cruz-Martin, J. Gonzalez, C. Galindo and J. L. Blanco, "Application of UWB and GPS technologies for vehicle localization in combined indoor-outdoor environments," 2007 9th International Symposium on Signal Processing and Its Applications, 2007, pp. 1-4, doi: 10.1109/ISSPA.2007.4555416.

[6] R. Faragher and R. Harle, “Location Fingerprinting With Bluetooth Low Energy Beacons,” *IEEE J. Sel. Areas Commun.*, vol. 33, no. 11, pp. 2418–2428, Nov 2015

[7] Euspa.europa.eu. 2022. *What is GNSS?*. [online] Available at: <https://www.euspa.europa.eu/european-space/eu-space-programme/what-gnss>

[8] “Bluetooth Low Energy (BLE) Beacon Technology Made Simple: A Complete Guide to

Bluetooth Beacons,"blog.beaconstac.com.https://blog.beaconstac.com/2018/08/ble-made-simple-a-complete-guide-to-ble- (accessed Sep. 28, 2022).

[9] S. Subedi, S.-S. Hwang, and J.-Y. Pyun, "Hybrid Wireless Indoor Positioning System Combining BLE Beacons And Wi-Fi APs," IEEE Xplore, Oct. 01, 2020. https://ieeexplore.ieee.org/abstract/document/9289235 (accessed Sep. 28, 2022).

[10] "What is a Beacon? The Complete Guide to Bluetooth Beacons," Kontakt.io. https://kontakt.io/what-is-a-beacon/

[11] Medium. 2020. Bluetooth Technology: What Has Changed Over The Years. [online]Available at: https://medium.com/jaycon-systems/bluetooth-technology-what-has-changed-over-the-years-385da7ec7154 [Accessed 17 May 2022].

[12] Bluetooth SIG. https://www.bluetooth.com/learn-about-bluetooth/tech-overview/ (Accessed 17 May 2022).

[13] "Angle of Arrival - Method for high-precision positioning," Mar. 03, 2020. https://www.favendo.com/angle-of-arrival (accessed Sep. 28, 2022).

[14] C. Sun, H. Zhao, L. Bai, J. W. Cheong, A. G. Dempster, and W. Feng, "GNSS-5G Hybrid Positioning Based on TOA/AOA Measurements," China Satellite Navigation Conference (CSNC) 2020 Proceedings: Volume III, pp. 527–537, 2020, doi: 10.1007/978-981-15-3715-8_47.

[15] "Global Navigation Satellite System (GNSS)," 2006. [Online]. Available: https://www.princeton.edu/~alaink/Orf467F07/GNSS.pdf

[16] "Satellite Navigation Systems - an overview | ScienceDirectTopics," www.sciencedirect.com. https://www.sciencedirect.com/topics/earth-and-planetary-sciences/satellite-navigation-systems

[17] "Sensors: The Role of GNSS (GPS)," ZAPT, Nov. 19, 2021. https://www.zaptllc.com/post/sensors-the-role-of-gnss-gps (accessed Sep. 28, 2022).

[18] L. Pan et al., "Satellite availability and point positioning accuracy evaluation on a global scale for integration of GPS, GLONASS, BeiDou and Galileo," Advances in Space Research, vol. 63, no. 9, pp. 2696–2710, May 2019, doi: 10.1016/j.asr.2017.07.029.

[19] "What is Pseudorange? - Spirent," www.spirent.com. https://www.spirent.com/blogs/2011-01-25_what_is_pseudorange

[20] “GNSS Shadow Matching: Improving GNSS positioning in Urban Canyons,” *Geoawesomeness*. https://geoawesomeness.com/eo-hub/gnss-shadow-matching-improving-gnss-positioning-urban-canyons/ (accessed Oct. 02, 2022).

[21] ”Coordinates,” James R. Clynch, Naval Postgraduate 2002 available: https://www.oc.nps.edu/oc2902w/coord/coord.pdf (accessed May. 27, 2022)

[22] “Comparison of 3-D Coordinate Systems - MATLAB & Simulink - MathWorks Nordic,” se.mathworks.com.https://se.mathworks.com/help/map/choose-a-3-d-coordinate-system.html (accessed Sep. 28, 2022).

[23] “Transformations between ECEF and ENU coordinates - Navipedia,” gssc.esa.int. https://gssc.esa.int/navipedia/index.php/Transformations_between_ECEF_and_ENU_coordinates (accessed Sep. 28, 2022).

[24] “What is Dilution of Precision? - everything RF,” Everythingrf.com, Mar. 11, 2022. https://www.everythingrf.com/community/what-is-dilution-of-precision

[25] Kaplan, E. and Hegarty, C. (2006) Understanding GPS Principles and Applications. 2nd Edition, Artech House Inc., Norwood, 332 p, 334 p.

[26] “XPLR-IOT-1,” u-blox, May 05, 2022. https://www.u-blox.com/en/product/xplr-iot-1?legacy=Current (accessed Sep. 28, 2022).

[27] “NINA-W15 series Stand-alone multiradio modules with Wi-Fi and Bluetooth Data sheet.” Accessed: Sep. 28, 2022. [Online]. Available: https://content.u-blox.com/sites/default/files/NINA-W15_DataSheet_UBX-18006647.p

[28] “NINA-B41 series (u-connect),” u-blox, Nov. 16, 2020. https://www.u-blox.com/en/product/nina-b41-series-u-connect (accessed Sep. 28, 2022).

[29] https//content.u-blox.com/sites/default/files/documents/ANT-B10_ProductSummary_UBX-21047856.pdf.

[30] “Radar Basics - Patch Antennas,” Radartutorial.eu, 2019. https://www.radartutorial.eu/06.antennas/Microstrip%20Antenna.en.html (accessed Dec. 16, 2019).

[31] ”Derivation of a constant Velocity Motion Model for Visual Tracking” Baisa, Nathanael L. (2020).

[32] F.Gustafsson, Statistical Sensor Fusion, 1st edition. Lund, 2010.